# MATHEMATICS OF MEDICAL IMAGING
## INVERTING THE RADON TRANSFORM

KAILEY BOLLES

Abstract. Computed Tomography (CT) and other radial imaging techniques are vital to the practice of modern medicine, allowing non-invasive examination of the inner workings of the human body. However, raw CT data must be transformed in order to become diagnostically relevant. This project examines raw CT data, modeled by the Radon transform, and methods of inversion via unfiltered backprojection, Fourier transforms, and filtered backprojection (the inverse Radon transform). We demonstrate this process through examples of "raw data" and inversion, with a focus on the influence of discrete data sets of different sizes on inversion quality.

## 1. Introduction

The study of medical imaging has led to techniques vital to the practice of medicine, such as x-ray imaging, computed tomography (CT) scans, magnetic resonance imaging, and a variety of other radiological imaging techniques. Such techniques allow the examination of the internal condition of the body without the use of invasive surgical procedures. Tomography, or slice imaging, represents a subset of these techniques, notably x-ray imaging and CT scans, used to translate two-dimensional external measurements into a reconstruction of three-dimensional internal structure. This investigation will focus on CT scans, although the mathematics of CT scans are very similar to those used in other types of medical imaging. CT scans are of particular practical interest because they are useful in diagnosing skeletal damage, cancers, and vascular diseases. They can also be used to guide surgery, biopsy, and radiation therapy in real time.

Many of the discussions found in this paper are adapted from Charles Epstein's *Introduction to the Mathematics of Medical Imaging* [1], Peter O'Neil's *Advanced Engineering Mathematics* [2], and Yves Nievergelt's *Elementary Inversion of Radon's Transform* [3]. These publications, particularly [1], also represent valuable sources for those desiring further information on these topics.

### 1.1. **X-Ray Imaging.**

X-ray imaging relies on the principle that an object will absorb or scatter x-rays of a particular energy in a manner dependent on its composition, quantified by the attenuation coefficient $\mu$. The attenuation coefficient $\mu$ of a substance is a function in $\mathbb{R}^3$ dependent on a variety of factors, but primarily reflective of the electron density of that substance. Therefore, denser substances and substances containing elements with many electrons will have higher attenuation coefficients. This helps explain why bone, which contains high percentages of calcium (20 electrons), potassium (19 electrons), phosphorous (15 electrons), and magnesium (12 electrons), has a much higher attenuation coefficient than soft tissue, which is made up primarily of carbon (6 electrons), nitrogen (7 electrons), and

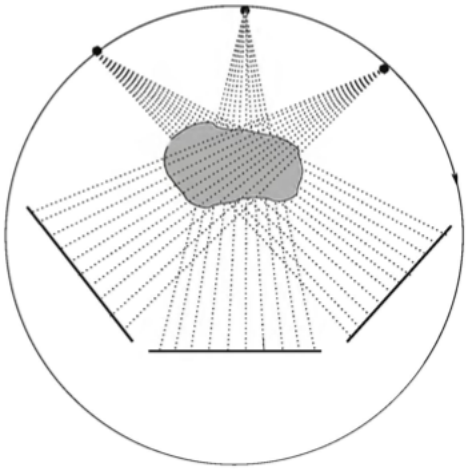

FIGURE 1. A 2D diagram of a CT scanner. The CT scanner is made up of a point-source emitter and film that rotate around an object of interest, imaging the object in 2D slices and then compiling these slices into a 3D rendering of the object. Image from [1].

oxygen (8 electrons) [1]. Air is considered to have an attenuation coefficient of zero for simplicity of calculation, so the attenuation coefficient disappears outside the body.

In practice, Hounsfield units–attenuation coefficients normalized to the attenuation coefficient of water–are used in favor of attenuation coefficients. This is due to the fact that these units are suited to the examination of organisms primarily composed of water, e.g., humans. The Hounsfield unit of a tissue is defined by

$$H_{tissue} = \frac{\mu_{tissue} - \mu_{water}}{\mu_{water}} \times 1000. \qquad \text{(from [1])}$$

Although this examination will focus on the mathematics of the attenuation coefficient itself, it is important to consider the practical ramifications represented by the Hounsfield unit representation of particular tissues. The typical clinical range of a CT scan, between air and bone, is approximately 2000 $H$ [1]. Soft tissue, the primary target of clinical investigation, represents a very small fraction of this range, meaning that CT scans must be extremely sensitive in order to be clinically useful.

1.2. **CT Scanning.** Computed tomography scanning is essentially an extrapolation of the concept of an x-ray. Instead of taking a single x-ray from a single perspective, a CT scan rotates a point source of x-rays around a body to be imaged. This exposes film on the opposite side of the object. By making calculations from the level of exposure (density) of the film, one can determine line integrals of the attenuation coefficient $\mu$ through the object. Taking the calculations from a full rotation, it is possible to reconstruct the 2D slice of the object. Compilation of multiple slices allows for 3D reconstruction of the object.

Essentially, the mathematics of CT scanning involves two problems. In the forward problem, we model the data obtained from real-world CT scans using the Radon transform. The Radon Transform allows us to create "film images" of objects that are very similar to those actually occurring in x-rays or CT scans. The inverse problem allows us to convert Radon transforms back into attenuation coefficients using the inverse Radon transform–to reconstruct the body from a CT scan.

1.3. **Thesis Objectives.** This thesis addresses both the forward and inverse problems of medical imaging and the Radon transform. Section 2 examines the parametrization and definition of the Radon transform, showing how we obtain the "mock CT" transform data by applying the Radon transform to known functions. A simple inversion technique called unfiltered backprojection–and its drawbacks–are examined in Section 3. Section 4 begins a discussion of another common data transform called the Fourier transform, which is linked to the Radon transform by the Central Slice Theorem discussed in Section 5. Sections 6 and 7 address methods of applying the Fourier transform to discrete, real-world data–the discrete Fourier transform and the sampled Fourier transform, respectively. An inversion formula for the Radon transform is presented and proved with calculus in Section 8. Section 9 presents a simple "body" as an example of moving through the process of Radon transform/CT data reconstruction and shows the effect of different levels of discrete data on reconstructions. The paper concludes and presents possibilities for further exploration in Section 10.

## 2. The Radon Transform

In order to work in the circular geometry of CT scans, it is helpful to parametrize lines $ax+by=c$ in $\mathbb{R}^2$ to a set of oriented lines with radial parameters $\ell_{t,\theta}$ in $\mathbb{R}\times S^1$ (see figure 2). In medical imaging, these lines are representative of the trajectories of x-ray beams entering a body. Consider the general line in $\mathbb{R}^2$

$$ax + by = c, \tag{1}$$

where $a$, $b$, and $c$ are constants. We then have

$$\frac{a}{\sqrt{a^2+b^2}}x + \frac{b}{\sqrt{a^2+b^2}}y = \frac{c}{\sqrt{a^2+b^2}}.$$

The first two coefficients, $\left(\frac{a}{\sqrt{a^2+b^2}}, \frac{b}{\sqrt{a^2+b^2}}\right)$, define a point on the unit circle. Let $\theta$ be the angle corresponding to that point on the unit circle, so

$$\theta = \cos^{-1}\left(\frac{a}{\sqrt{a^2+b^2}}\right).$$

Then $\cos\theta = \frac{a}{\sqrt{a^2+b^2}}$ and $\sin\theta = \frac{b}{\sqrt{a^2+b^2}}$. This parametrization has an intrinsic repetitive quality; the angle $\theta$ can only take on values of $[0,\pi)$ before repeating previously described lines. Let $t$ be the distance from the origin to the line $ax+by=c$ along the angle $\theta$. Then the line can also be described as the set of solutions $(x,y)$ to the inner product

$$t = \langle (x,y), (\cos\theta, \sin\theta)\rangle = \langle (x,y), \omega\rangle.$$

Therefore, $t$ is equal to the right side of equation (1). Notice that our definitions of $t$ and $\theta$ also give us a point on the line, $(t\cos\theta, t\sin\theta)$, where a line at angle $\theta$

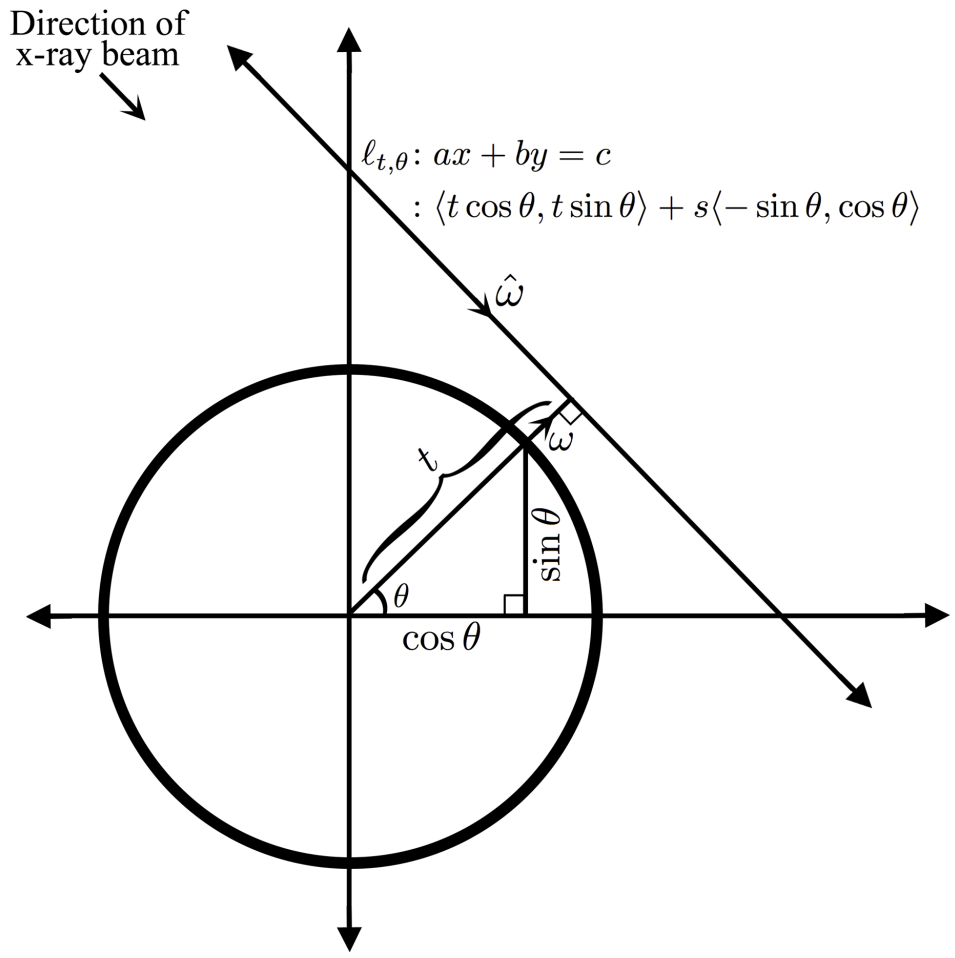


FIGURE 2. The parametrization of lines $ax + by = c$ to lines $\ell_{t,\theta}$ in $\mathbb{R}^2$.

intersects $ax + by = c$. This intersection is a right angle, because while the slope of the line $ax + by = c$ is $-\frac{a}{b}$, the tangent of $\theta$ is

$$\tan\theta = \frac{\sin\theta}{\cos\theta} = \frac{b}{a}.$$

Let the vector $\omega = \langle\cos\theta, \sin\theta\rangle$, perpendicular to the line $ax + by = c$, and let the vector $\hat{\omega} = \langle -\sin\theta, \cos\theta\rangle$ be parallel to this line. We can therefore create a vector equation in terms of $t$ and $\theta$ for the line,

$$\begin{aligned} \ell_{t,\theta} &= t\omega + s\hat{\omega} \\ &= \langle t\cos\theta, t\sin\theta\rangle + s\langle -\sin\theta, \cos\theta\rangle, \end{aligned}$$

where $s \in \mathbb{R}$. This line is the same as the line $ax + by = c$, but the parametrization is in terms of an affine parameter $t$ and the angular parameter $\theta$, making it easier to determine a set of lines emanating from or passing through a single point.

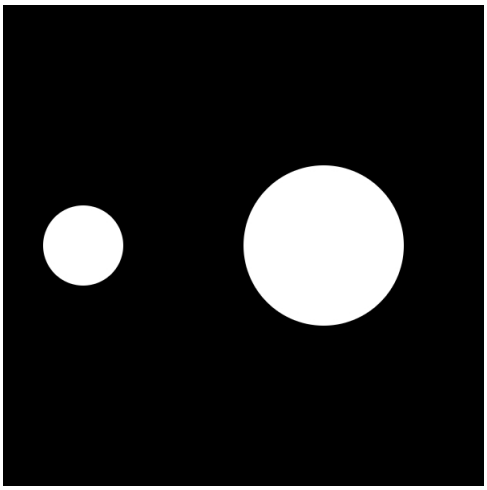

FIGURE 3. The piecewise-defined function $g$.

**Definition 2.1.** *Let $f$ be some function in $\mathbb{R}^2$, parametrized over the lines $\ell_{t,\theta}$. The **Radon transform** $\mathscr{R}f(t,\theta)$ is defined as*

$$\mathscr{R}f(t,\theta) = \int_{\ell_{t,\theta}} f ds = \int_{-\infty}^{\infty} f(t\omega + s\hat{\omega}) ds = \int_{-\infty}^{\infty} f(t\cos\theta - s\sin\theta, t\sin\theta + s\cos\theta) ds.$$

This definition describes the Radon transform for an angle $\theta$. These discrete-$\theta$ Radon transforms can be combined, taking the integral of a function $f$ over *all* lines $\ell_{t,\theta}$ in $\mathbb{R}\times S^1$. For our purposes, it accurately models the data acquired from taking cross-sectional scans of an object from a large set of angles, as in CT scanning, and its inverse can be used to reconstruct an object from CT data.

To illustrate this process, consider the following simple example function

$$g(x,y) = \begin{cases} 1 & (x-1)^2 + y^2 \leq 1 \\ 1 & (x+2)^2 + y^2 \leq \frac{1}{4} \\ 0 & \text{everywhere else,} \end{cases}$$

shown in figure 3.

Taking the Radon transform $\mathscr{R}$ for discrete values of $\theta$, we acquire a set of "line profiles" of the intensity of $g$ at an angle perpendicular to the angle $\theta$ (see figure 4). These profiles are perpendicular due our initial parametrization, in which the line of interest $\ell_{t,\theta}$ is perpendicular to the vector $\langle\cos\theta, \sin\theta\rangle$.

The Radon transform $\mathscr{R}$ of the function $g$, plotted over all values of $t$ and $\theta$, can be seen in figure 5. This image represents a collection of all of the possible discrete Radon transforms (such as those shown in figure 4), where the axes represent the $t$ and $\theta$ values and the color brightness represents the intensity/density of the function (the vertical scale of figure 4) at a particular point.

## 3. Unfiltered Backprojection

The Radon transform is helpful to tomography applications such as CT because it can model the data originally obtained from such scans. However, such data is not immediately applicable to diagnostic applications because it does not directly

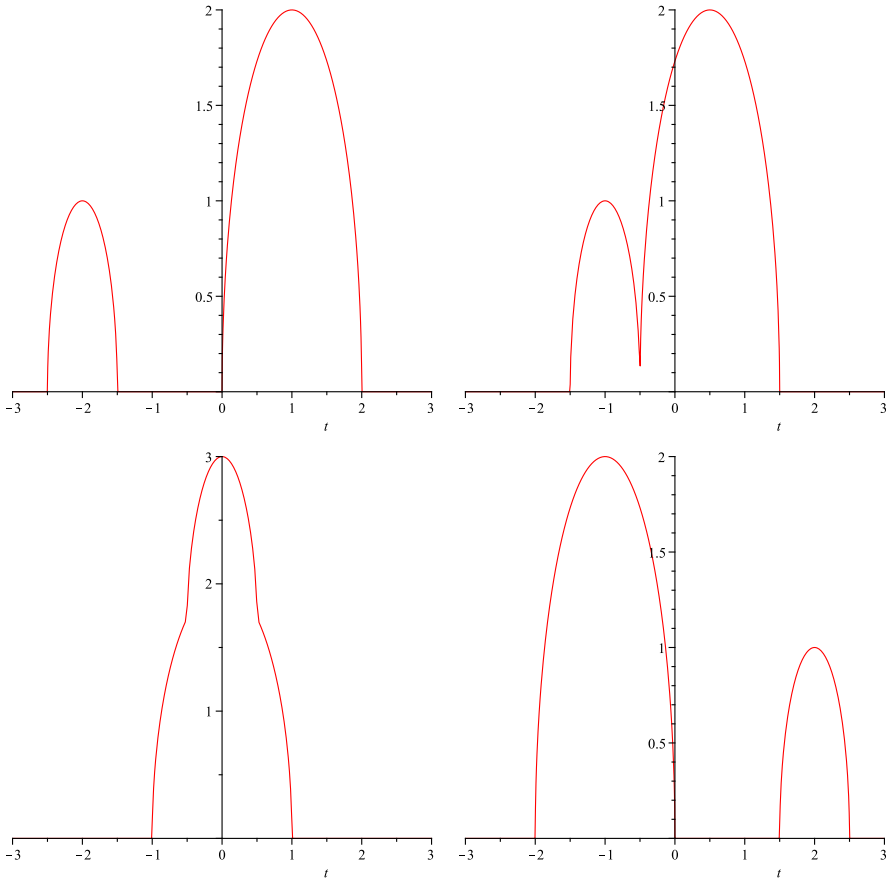


FIGURE 4. Radon transform $\mathscr{R}(g)$ of the piecewise-defined function $g$ at the angles $\theta = 0$ (upper left), $\theta = \frac{\pi}{3}$ (upper right), $\theta = \frac{\pi}{2}$ (lower left), and $\theta = \pi$ (lower right). Note that in this parametrization, the angle $\theta$ is perpendicular to the angle of the line passing through the object. Image created using Maple.

resemble the object being imaged. A method of recreating the original image (in the case of the Radon transform itself, the original function) with a high degree of specificity and veracity is therefore required in order to apply tomographic technologies in the real world. Perfect reconstruction via abstract inversion is possible for continuous data (i.e., functions) but the finite (discrete) data available in the real world allows for only estimated reconstructions. Thus most work for CT and other real-world applications focuses on improving these estimates.

An initially appealing method is unfiltered backprojection, which takes the average values of the function along each line and "smears" or projects them back over the line in order to create an image.

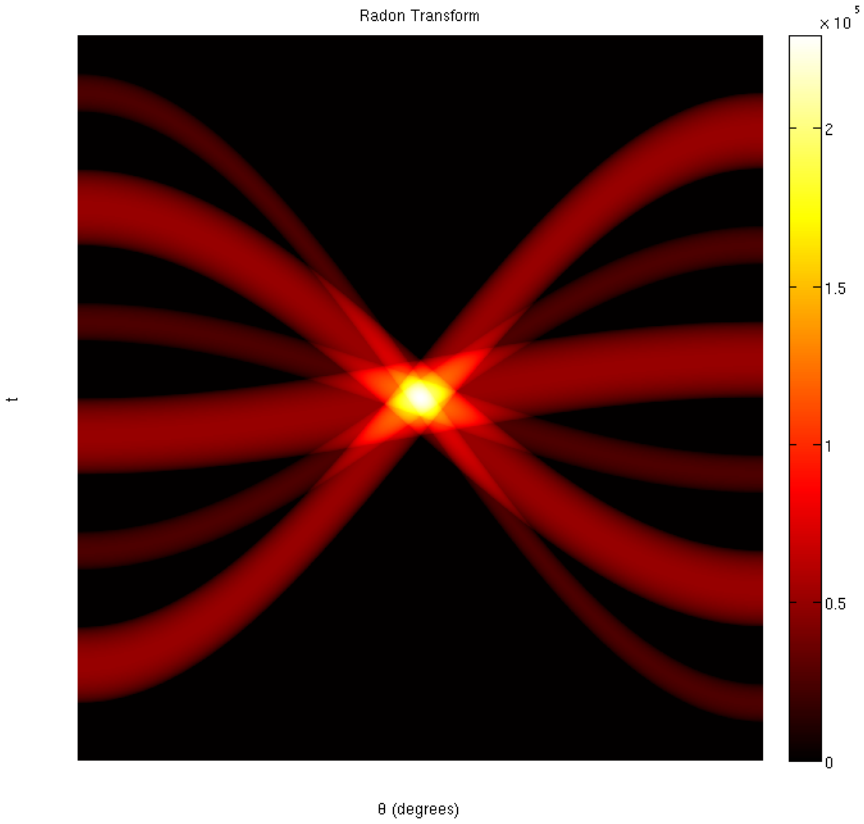


FIGURE 5. The Radon transform of the function $g$ over all values of $t$ and $\theta$. The brightness of the image represents the "density" of the function $g$ at a particular point. Image created using MATLAB.

**Definition 3.1** (from [1]). *Let $f$ be some function in $\mathbb{R}^2$, parametrized over the lines $\ell_{t,\theta}$. The* ***unfiltered backprojection*** *$B[f(t,\theta)]$ is defined as*

$$B[f(t,\theta)] = \frac{1}{2\pi}\int_0^{2\pi} \mathscr{R}f(t,\theta)d\theta.$$

Unfiltered backprojection is a simple and logical computation, but not a faithful representation of $f$, as can be observed in the graphs of the two-circle example function $g$ and its unfiltered backprojection in figure 6. The unfiltered backprojection retains the basic characteristics of $g$, but it loses contrast and introduces imaging artifacts (i.e., radial blur). This is not particularly problematic for a simple, high contrast image like the example function $g$. However, in medical applications where the areas of interest are likely soft tissues with highly similar attenuation coefficients, loss of contrast and introduction of imaging artifacts would likely render an image completely useless. Therefore unfiltered backprojection is not a viable

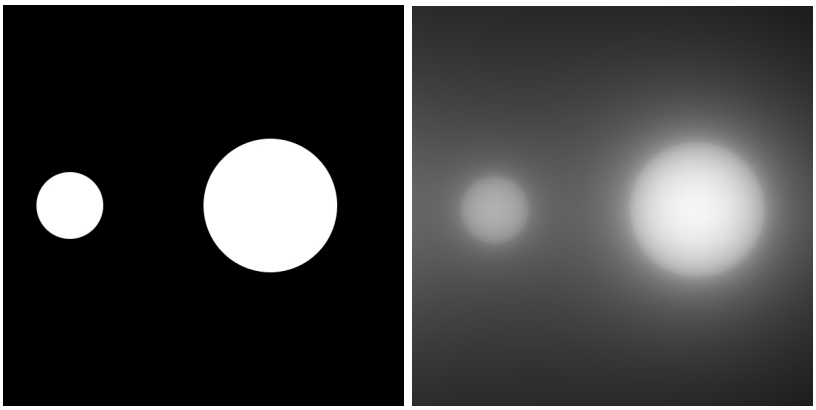

FIGURE 6. The example function $g$ (left) and its unfiltered backprojection (right). Backprojection created using MATLAB.

solution to the problem of inverting the Radon transform for medical imaging applications.

As unfiltered backprojection's lack of specificity renders it unusable for medical imaging applications, we must examine other methods for inverting the Radon transform. The Radon transform is closely related to the Fourier transform, an extensively studied method whose inverse is well-described, by the Central Slice Theorem. We will introduce the Fourier transform before exploring this relationship further. Derivations and notation for this section will closely follow [2].

## 4. Fourier Transform Derivation

Suppose a function $f$ is absolutely integrable, that is, that $\int_{-\infty}^{\infty} |f(x)|dx$ converges and $f$ is piecewise smooth on every interval $[-L, L]$. Then the Fourier series for $f$ on this arbitrary interval is

$$\begin{aligned} FS[f(\upsilon)] &= \frac{1}{2L}\int_{-L}^{L} f(\upsilon)d\upsilon + \sum_{n=1}^{\infty}\left(\frac{1}{L}\int_{-L}^{L} f(\upsilon)\cos\left(\frac{n\pi\upsilon}{L}\right)d\upsilon\right)\cos\left(\frac{n\pi x}{L}\right) + \\ &\quad + \sum_{n=1}^{\infty}\left(\frac{1}{L}\int_{-L}^{L} f(\upsilon)\sin\left(\frac{n\pi\upsilon}{L}\right)d\upsilon\right)\sin\left(\frac{n\pi x}{L}\right). \end{aligned}$$

To simplify these equations, let $\omega_n = \frac{n\pi}{L}$ and $\omega_n - \omega_{n-1} = \frac{\pi}{L} = \Delta\omega$, so that $\omega$ becomes angular frequency and conveniently absorbs the angular terms of the Fourier series. Then the Fourier series of $f$ becomes

$$\begin{aligned} FS[f(\upsilon)] &= \frac{1}{2\pi}\left(\int_{-L}^{L} f(\upsilon)d\upsilon\right)\Delta\omega + \frac{1}{\pi}\sum_{n=1}^{\infty}\left(\int_{-L}^{L} f(\upsilon)\cos(\omega_n\upsilon)d\upsilon\right)\cos(\omega_n x)\Delta\omega + \\ &\quad + \frac{1}{\pi}\sum_{n=1}^{\infty}\left(\int_{-L}^{L} f(\upsilon)\sin(\omega_n\upsilon)d\upsilon\right)\sin(\omega_n x)\Delta\omega. \end{aligned} \tag{2}$$

In order to get an approximation for the whole real line, let us examine the Fourier series of $f$ as $L$ approaches infinity. Letting $L$ approach infinity causes $\Delta\omega$ to

approach zero. The first component of equation (2) will therefore also approach zero, that is,

$$\text{as} \qquad \Delta\omega \to 0, \qquad \frac{1}{2\pi}\left(\int_{-L}^{L} f(\upsilon)d\upsilon\right)\Delta\omega \to 0,$$

because we assumed that $f$ was absolutely convergent. Therefore, equation (2) approaches

$$\frac{1}{\pi}\int_0^\infty \left[\left(\int_{-\infty}^{\infty} f(\upsilon)\cos(\omega\upsilon)d\upsilon\right)\cos(\omega x) + \left(\int_{-\infty}^{\infty} f(\upsilon)\sin(\omega\upsilon)d\upsilon\right)\sin(\omega x)\right]d\omega,$$

as $L$ approaches infinity. This is the Fourier integral of $f$ on the real line. If $f$ is continuous at $x$, this integral converges to $f(x)$. If there is a jump discontinuity in $f$, the integral will return the average of the values of the function $\lim_{x\to a^-} f(x)$ and $\lim_{x\to a^+} f(x)$ on either side of the jump. Using trigonometric identities, the Fourier integral can also be expressed as

$$FI[f(\upsilon)] = \frac{1}{\pi}\int_0^\infty \int_{-\infty}^{\infty} f(\upsilon)\cos(\omega(\upsilon - x))d\upsilon d\omega.$$

The complex form of the cosine function in this case is

$$\cos(\omega(\upsilon - x)) = \frac{1}{2}\left(e^{\mathrm{i}\omega(\upsilon - x)} + e^{-\mathrm{i}\omega(\upsilon - x)}\right).$$

If we insert this complex form into the Fourier integral, we eventually find that

$$FI[f(\upsilon)] = \frac{1}{2\pi}\int_{-\infty}^{\infty} Ce^{\mathrm{i}\omega x}d\omega,$$

where $C = \int_{-\infty}^{\infty} f(t)e^{-\mathrm{i}\omega t}dt$. This is the complex Fourier integral of $f$, and its coefficient $C$ is the Fourier transform of $f$, also written as $\hat{f}(\omega)$.

**Definition 4.1.** *Let $f(x)$ be an absolutely integrable function with frequency $\omega$. Then the **Fourier transform** $\hat{f}(\omega)$ (also written as $\mathcal{F}[f(x)](\omega)$) is defined as*

$$\hat{f}(\omega) = \int_{-\infty}^{\infty} f(x)e^{-\mathrm{i}\omega x}dx.$$

**Definition 4.2.** *Let $F(\omega)$ be an absolutely integrable function. Then the **inverse Fourier transform** $\check{f}(x)$ (also written as $\mathcal{F}^{-1}[F(\omega)](x)$) is defined as*

$$\check{f}(x) = \mathcal{F}^{-1}[F(\omega)](x) = \frac{1}{2\pi}\int_{-\infty}^{\infty} \hat{f}(\omega)e^{\mathrm{i}\omega x}d\omega.$$

Consider the case where $F(\omega)$ is an absolutely integrable Fourier transform of a function that is also absolutely integrable. If both functions satisfy estimates of the form

$$|F(\omega)| \le \frac{Q}{(1 + ||\omega||)^{1+\delta}} \qquad \text{for a} \qquad \delta > 0,$$
$$|f(x)| \le \frac{P}{(1 + ||x||)^{1+\epsilon}} \qquad \text{for an} \qquad \epsilon > 0,$$

where $P$ and $Q$ are upper limits on both the functions and their derivatives, then the inverse Fourier transform of the Fourier transform $F(\omega)$ of $f(x)$ will equal the original function $f(x)$,

$$\check{\hat{f}}(x) = \mathcal{F}^{-1}\left[\mathcal{F}[f(x)](\omega)\right](x) = f(x).$$

In order to work in two-dimensional CT geometry, it is helpful to include an extension of the Fourier transform into two dimensions. Its derivation is similar, but considers two angular frequencies $r$ and $\omega$, operating in the two different directions of the plane.

**Definition 4.3.** *Let $f(x, y)$ be an absolutely integrable function. Then the **two-dimensional Fourier transform** $\hat{f}(r, \omega)$ is defined as*

$$\hat{f}(r, \omega) = \int_{-\infty}^{\infty} \int_{-\infty}^{\infty} f(x, y) e^{-\mathrm{i}r\omega \cdot \langle x, y \rangle} dx dy.$$

## 5. Central Slice Theorem

Having defined both the Radon transform and the Fourier transform, we can now explore the Central Slice Theorem, which connects the two transforms. This discussion closely parallels that found in [1].

**Theorem 5.1.** *Let the natural domain of $\mathscr{R}$ be defined as those functions which are piecewise continuous and satisfy an estimate of the form*

$$|f(\xi)| \leq \frac{Q}{(1 + ||\xi||)^{1+\epsilon}} \qquad \text{for an} \qquad \epsilon > 0,$$

*where $\xi = t\omega + s\hat{\omega}$ and $Q$ is an upper limit on both the Radon transform and its derivative. Let $f$ be an absolutely integrable function in this domain. For any real number $r$ and unit vector $\omega = \langle \cos\theta, \sin\theta \rangle$, we have the identity*

$$\int_{-\infty}^{\infty} \mathscr{R}f(t, \theta) e^{-\mathrm{i}tr} dt = \hat{f}(r, \omega).$$

*Proof.* Begin by substituting the definition of $\mathscr{R}$ into the first statement of the identity to obtain

$$\int_{-\infty}^{\infty} \mathscr{R}f(t, \theta) e^{-\mathrm{i}tr} dt = \int_{-\infty}^{\infty} \int_{-\infty}^{\infty} f(t\omega + s\hat{\omega}) e^{-\mathrm{i}tr} ds dt,$$

where $\hat{\omega} = \langle -\sin\theta, \cos\theta \rangle$, the vector perpendicular to $\omega$. Performing the change of variables $\xi = t\omega + s\hat{\omega}$ we find

$$\begin{aligned} \int_{-\infty}^{\infty} \int_{-\infty}^{\infty} f(t\omega + s\hat{\omega}) e^{-\mathrm{i}tr} ds dt &= \int_{\mathbb{R}^2} f(\xi) e^{-\mathrm{i}tr} d\xi \\ &= \int_{-\infty}^{\infty} \int_{-\infty}^{\infty} f(x, y) e^{-\mathrm{i}r\omega \cdot \langle x, y \rangle} dx dy \\ &= \hat{f}(r, \omega). \quad \square \end{aligned}$$

Therefore, the two-dimensional Fourier transform $\hat{f}(r, \omega)$ is the one-dimensional Fourier transform of $\mathscr{R}f(t, \theta)$.

In order to better understand how the two-dimensional Fourier transform $\hat{f}(r, \omega)$ is equivalent to the one-dimensional Fourier transform of $\mathscr{R}f(t, \theta)$, let us consider an example. Let $\theta = 0$ so that $\omega = (\cos\theta, \sin\theta)$ becomes the unit vector (1,0) and

$\hat{\omega}$ is the unit vector (0,1), perpendicular to $\omega$. The Radon transform $\mathscr{R}f(t,\theta)$ is then

$$\begin{aligned}\mathscr{R}f(t,\theta) &= \int_{-\infty}^{\infty} f\left(t\omega + s\hat{\omega}\right) ds \\ &= \int_{-\infty}^{\infty} f\left(t\cdot(1,0) + s\cdot(0,1)\right) ds \\ &= \int_{-\infty}^{\infty} f\left(t,s\right) ds.\end{aligned}$$

Then the Fourier transform of $\mathscr{R}f(t,\theta)$ is

$$\int_{-\infty}^{\infty} \mathscr{R}f(t,\theta)e^{-\mathrm{i}rt}dt = \int_{-\infty}^{\infty}\int_{-\infty}^{\infty} f(t,s)e^{-\mathrm{i}rt}dsdt,$$

where $r$ is a constant. Since the inner product $\langle r\omega,(t,s)\rangle = rt$, the last statement is the definition of the two-dimensional Fourier transform $\hat{f}(r,\omega)$.

## 6. Discrete Fourier Transform

In medical imaging, we are not working with continuous inputs (e.g., functions or infinite data sets) but with discrete ones (e.g., real-world, finite data). Therefore we cannot directly apply the Central Slice Theorem and Fourier transform, because it applies to *continuous* data. We need a method for modeling the Fourier transform of discrete data: the discrete Fourier transform.

**Definition 6.1** (from [2])**.** *(from* [1]*) Let $u = \{u_j\}_{j=0}^{N-1}$ be a sequence of $N$ complex numbers. Then the* ***N-point discrete Fourier transform*** *$\mathbb{D}[u]$ is given by*

$$\mathbb{D}[u](k) = U_k = \sum_{j=0}^{N-1} u_j e^{-2\pi\mathrm{i}jk/N},$$

*where $k = 0, \pm1, \pm2, ...$*

**Theorem 6.1.** *Let $\mathbb{D}[u](k)$ be an $N$-Point discrete Fourier transform. Then the* ***inverse discrete Fourier transform*** *can be used to recover the sequence $u = \{u_j\}_{j=0}^{N-1}$ of $N$ complex numbers upon which $\mathbb{D}[u](k)$ is based. Each $u_j$ in the sequence is given by*

$$u_j = \frac{1}{N}\sum_{k=0}^{N-1} U_k e^{2\pi\mathrm{i}jk/N},$$

*for $j = 0, 1, ..., N-1$.*

In order to prove this assertion, let us first set a variable $W = e^{2\pi\mathrm{i}/N}$. Observe that $W$ has the properties that

$$W^N = 1 \qquad \text{and} \qquad W^{-1} = e^{-2\pi\mathrm{i}/N}.$$

This makes $W$ a very convenient substitution to use in the Inverse discrete Fourier transform, as

$$\frac{1}{N}\sum_{k=0}^{N-1} U_k e^{-2\pi\mathrm{i}jk/N} = \frac{1}{N}\sum_{k=0}^{N-1} U_k W^{-jk}.$$

We can make a substitution for $U_k$ using our initial definition of the $N$-Point discrete Fourier transform in definition 6.1, giving us

$$\frac{1}{N}\sum_{k=0}^{N-1} U_k W^{-jk} = \frac{1}{N}\sum_{k=0}^{N-1}\left(\sum_{m=0}^{N-1} u_m e^{-2\pi \mathrm{i} mk/N}\right) W^{-jk}.$$

The variable $W$ once again comes in useful as a substitution here, allowing us to convert the equation to

$$\frac{1}{N}\sum_{k=0}^{N-1}\left(\sum_{m=0}^{N-1} u_m e^{-2\pi \mathrm{i} mk/N}\right) W^{-jk} = \frac{1}{N}\sum_{k=0}^{N-1}\sum_{m=0}^{N-1} u_m W^{mk} W^{-jk}.$$

We can then change the order of summation to isolate our $W$ terms, as in

$$\frac{1}{N}\sum_{k=0}^{N-1}\sum_{m=0}^{N-1} u_m W^{mk} W^{-jk} = \frac{1}{N}\sum_{m=0}^{N-1} u_m \sum_{k=0}^{N-1} W^{mk} W^{-jk}. \tag{3}$$

This equation can be simplified by examining the properties of the $W$ terms of the last sum. First observe that

$$W^{mk}W^{-jk} = e^{-2\pi \mathrm{i} mk/N} e^{2\pi \mathrm{i} jk/N} = e^{-2\pi \mathrm{i}(m-j)k/N} = W^{(m-j)k}.$$

The value of this final term depends on the values of $m$ and $j$. If, for a given $j$, $m \neq j$, then

$$\sum_{k=0}^{N-1} W^{mk}W^{-jk} = \sum_{k=0}^{N-1} W^{(m-j)k} = \sum_{k=0}^{N-1} \left(W^{m-j}\right)^k.$$

This is recognizable as the finite sum of a geometric series, and we can therefore apply the equation for the finite sum of a geometric series,

$$\sum_{i=0}^{n} \alpha^i = \frac{1-\alpha^{n+1}}{1-\alpha},$$

to find that

$$\sum_{k=0}^{N-1} \left(W^{m-j}\right)^k = \frac{1-\left(W^{m-j}\right)^N}{1-W^{m-j}}.$$

Observe that from our definition of $W$, $\left(W^{m-j}\right)^N = e^{-2\pi \mathrm{i}(m-j)} = 1$ (because $m-j$ must be some integer value) and $W^{m-j} = e^{-2\pi \mathrm{i}(m-j)/N} \neq 1$. Therefore, when $m \neq j$

$$\sum_{k=0}^{N-1} W^{mk}W^{-jk} = \frac{1-\left(W^{m-j}\right)^N}{1-W^{m-j}} = 0.$$

If $m = j$, however, then

$$\sum_{k=0}^{N-1} W^{mk}W^{-jk} = \sum_{k=0}^{N-1} W^{jk}W^{-jk} = \sum_{k=0}^{N-1} 1 = N.$$

Therefore we only need to keep the term when $r = j$ in the summation with respect to $r$ in equation (3), giving us

$$\frac{1}{N}\sum_{m=0}^{N-1} u_m \sum_{k=0}^{N-1} W^{mk}W^{-jk} = \frac{1}{N}u_j \sum_{k=0}^{N-1} W^{jk}W^{-jk} = \frac{1}{N}u_j N = u_j$$

and thereby proving the formula for the inverse $N$-Point discrete Fourier transform.

## 7. Sampled Fourier Transform

The discrete Fourier transform allows us to approximate the Fourier coefficients of a periodic function $f$. We can apply this knowledge, and specifically the knowledge of the inverse $N$-point Fourier transform, to approximate the sampled partial sums of the Fourier series of a periodic function like the Radon transform, thereby modeling the Fourier series of the function with a discrete set of samples.

To derive the sampled Fourier transform, let us first consider the partial sum over the interval $[0, p]$

$$S_M(t) = \sum_{k=-M}^{M} d_k e^{2\pi \mathrm{i} kt/p}. \tag{4}$$

where $d_k$ are the discrete $\hat{f}$ coefficients and $M$ are the summation endpoints. Subdivide the interval $[0, p]$ into $N$ subintervals and choose the sample points $t_j = \frac{jp}{N}$. Form an $N$-point sequence of sampled points $u = \left\{f(\frac{jp}{N})\right\}_{j=0}^{N-1}$. Drawing on what we now know from the $N$-point Fourier transform and its inverse, we can estimate

$$d_k \approx \frac{1}{N} U_k \qquad \text{where} \qquad U_k = \sum_{j=0}^{N-1} f\left(\frac{jp}{N}\right) e^{-2\pi \mathrm{i} jk/N}.$$

In order to keep the sampled Fourier transform approximation within tolerable error ranges, we must constrain $k$, the number of Fourier coefficients estimated. This is necessary because while $U_k$ is periodic of period $N$, the values of the discrete $\hat{f}$ coefficients $d_k$ are not. For some $k$, it is possible that $U_k$ can be exactly equal to $d_k$, but due to the different periodicity properties this cannot hold true for all $k$, and the divergence from the nonperiodic $d_k$ values will become larger as $k$ increases. Therefore, we constrain $|k|$ to be less than or equal to $\frac{N}{8}$, an empirically derived constraint that approximates $d_k$ to within an acceptable tolerance for most science and engineering applications [2].

Due to the constraint that $|k| \leq \frac{N}{8}$, we set the bounds $M$ on $k$ in equation (4) such that $M \leq \frac{N}{8}$, so

$$S_M(t) \approx \sum_{k=-M}^{M} \frac{1}{N} U_k e^{2\pi \mathrm{i} kt/p}.$$

If we sample this sum at our partition points $t_j = \frac{jp}{N}$, then

$$S_M\left(\frac{jp}{N}\right) \approx \frac{1}{N} \sum_{k=-M}^{M} U_k e^{2\pi \mathrm{i} jk/N}.$$

This sum is the $N$-point inverse discrete Fourier transform for some $N$-point sequence.

We can use the periodicity of the $N$-point discrete Fourier transform ($U_{k+N} = U_k$) to find that

$$S_M\left(\frac{jp}{N}\right) \approx \frac{1}{N} \sum_{k=-M}^{-1} U_k e^{2\pi \mathrm{i} jk/N} + \frac{1}{N} \sum_{k=0}^{M} U_k e^{2\pi \mathrm{i} jk/N}.$$

Modifying the indices of summation, this becomes

$$S_M\left(\frac{jp}{N}\right) \approx \frac{1}{N}\sum_{k=N-M}^{N-1} U_k e^{2\pi \mathrm{i} jk/N} + \frac{1}{N}\sum_{k=0}^{M} U_k e^{2\pi \mathrm{i} jk/N} \tag{5}$$

The summations in equation (5) use the $2M+1$ numbers $U_{N-M}, ...U_{N-1}, U_0, ...U_M$.

This method can be used to more generally approximate a Fourier series $\hat{f}(\omega)$ over a finite interval $[0, 2\pi L]$. Suppose that $\hat{f}(\omega)$ can be approximated within an acceptable tolerance, the definition of "acceptable" depending on application, by an integral over the interval $[0, 2\pi L]$, that is, that

$$\hat{f}(\omega) = \int_{-\infty}^{\infty} f(x) e^{-\mathrm{i}\omega x} dx \approx \int_{0}^{2\pi} f(x) e^{-\mathrm{i}\omega x} dx. \tag{6}$$

If we subdivide $[0, 2\pi L]$ into $N$ subintervals of length $\frac{2\pi L}{N}$ and choose partition points $x_j = \frac{2\pi jL}{N}$, where $j = 0, 1, ..., N$, then the last integral in equation (6) can be estimated by

$$\hat{f}(\omega) \approx \sum_{j=0}^{N-1} \left(\frac{2\pi jL}{N}\right) f\left(\frac{2\pi jL}{N}\right) e^{-2\pi \mathrm{i} jL\omega/N}.$$

If we let $\omega = \frac{k}{L}$, where $k$ is any integer, then we find that

$$\hat{f}\left(\frac{k}{L}\right) \approx \sum_{j=0}^{N-1} \left(\frac{2\pi jL}{N}\right) f\left(\frac{2\pi jL}{N}\right) e^{-2\pi \mathrm{i} jk/N}.$$

This sampled Fourier transform is periodic of period $N$, but the actual values of $\hat{f}\left(\frac{k}{L}\right)$ are not, and so we again set the restriction that $|k| \leq \frac{N}{8}$.

For example, consider the function

$$h(t) = \begin{cases} e^{-t} & \text{for } t \geq 0, \\ 0 & \text{for } t < 0. \end{cases}$$

To approximate $\hat{h}\left(\frac{k}{L}\right)$ with a sampled Fourier transform, we (arbitrarily) choose $L = 1$, $N = 2^7 = 128$. The sampled Fourier transform of $h$ is therefore given by the equation

$$\hat{h}\left(\frac{k}{L}\right) \approx \frac{\pi}{64}\sum_{j=0}^{127} e^{-\pi j/64} e^{-\pi \mathrm{i} jk/64}.$$

Choosing a value of $k$ such that $\frac{k}{L} = 3$, we can calculate this approximation to find that

$$\begin{aligned} \hat{h}(3) &\approx \frac{\pi}{64}\sum_{j=0}^{127} e^{-\pi j/64} e^{-\pi \mathrm{i} jk/64} \\ &\approx 0.12451 - 0.29884\mathrm{i}. \end{aligned} \tag{7}$$

The Fourier transform of $h(t)$ is

$$\begin{aligned}\hat{h}(\omega) &= \int_{-\infty}^{\infty} h(\xi)e^{-\mathrm{i}\omega\xi}d\xi \\ &= \int_{0}^{\infty} e^{-\xi}e^{-\mathrm{i}\omega\xi}d\xi \\ &= \frac{1-\mathrm{i}\omega}{1+\omega^2}\end{aligned}$$

The Fourier transform for $k = 3$ is therefore

$$\hat{h}(3) = \frac{1-3\mathrm{i}}{10} = 0.1 - 0.3\mathrm{i}.$$

Comparing this to the result of the sampled Fourier series in equation (7), we can see that these results are remarkably similar. We could achieve an even more precise modeling of $\hat{h}\left(\frac{k}{L}\right)$ by choosing a larger value for $N$, but the calculations would require more time and computing power. Balancing between the precision of these calculations and the time taken to achieve them is vital to their uses in science and engineering, because too many calculations can quickly become prohibitive.

If we calculate the sampled Fourier series for a several values of $k$, it is possible for us to make a graphical model of $\hat{h}\left(\frac{k}{L}\right)$. Figure 7 shows the Fourier transform and the sampled Fourier series of $h(t)$ for $k = 0, ..., 15$. The sampled Fourier series are not in perfect agreement with the actual Fourier transform, but they do capture the "general trend" of $\hat{h}\left(\frac{k}{L}\right)$.

## 8. The Radon Inversion Formula

The inverse Radon transform is a technique used to reconstruct a function on the plane from its integrals over all lines in the plane. This provides a solution to the problem of reconstructing an image of the body from CT scan data. Several methods for inverting the Radon transform exist, some of which use Fourier transforms, the Central Slice Theorem, and functional analysis. However, in "Elementary Inversion of Radon's Transform" ([3]) Yves Nievergelt demonstrates proofs of this formula using only calculus and basic linear algebra, though the other mathematics exist as deeper, tacit portions of the formula and proof.

In essence, this formula takes unfiltered backprojection a step further. Instead of simply averaging the Radon transform over a line and "smearing" it to obtain a result, the inverse Radon transform $\mathscr{R}^{-1}$ (also called "filtered backprojection") essentially applies an auxiliary filtering function, $\Gamma_z$, dependent upon $t$.

**Definition 8.1** (from [3])**.** *Given any integrable function $F$ of $t$ and $\theta$, the transform $\mathscr{R}^*$ defines a function in $x$ and $y$*

$$\mathscr{R}^*F(x,y) := \frac{1}{\pi}\int_0^{\pi} F\left(x\cos\theta + y\sin\theta, \theta\right) d\theta.$$

*The **adjoint** $\mathscr{R}^*F(x,y)$ is equal to the average of $F(t,\theta)$ over the lines $\ell_{t,\theta}$ passing through the point $(x,y)$.*

The relationship between the Radon transform $\mathscr{R}$ and its adjoint $\mathscr{R}^*$ is very similar to that between the scalar product of vectors and a matrix and its transpose.

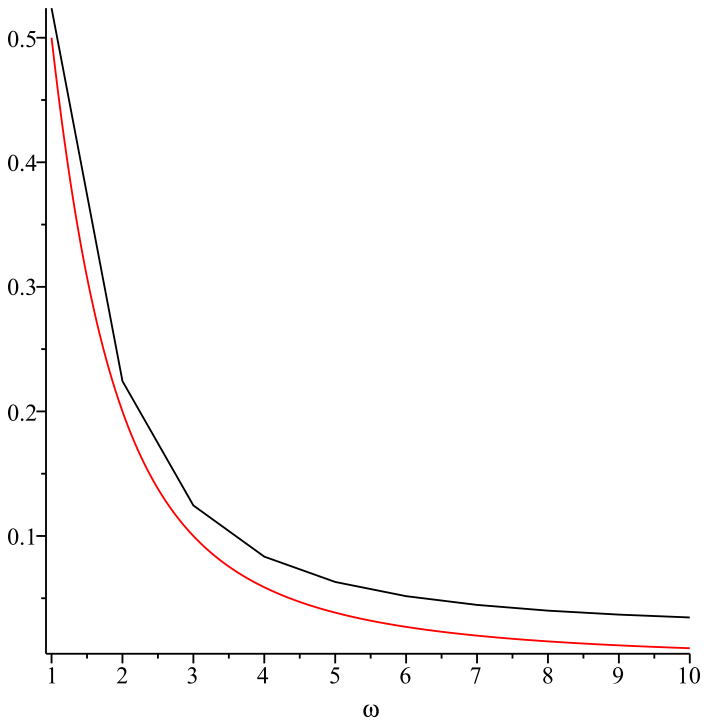


FIGURE 7. The sampled Fourier series (black) and Fourier transform (red) of the function $h$. Image created using Maple.

If we consider a continuous function $f$ equal to zero outside some disc and an integrable function $F$ of $t$ and $\theta$, then

$$\langle \mathscr{R}f, F\rangle = \langle f, \mathscr{R}^* F\rangle.$$

*Proof.* First consider the inner product of the Radon transform $\mathscr{R}$ and a function $F$, both of which are in the space of $(t,\theta)$, such that

$$\langle \mathscr{R}f, F\rangle = \frac{1}{\pi}\int_0^\pi \int_{-\infty}^{\infty} \mathscr{R}f(t,\theta)F(t,\theta)dtd\theta.$$

Substituting in the definition of the Radon transform, find that

$$\langle \mathscr{R}f, F\rangle = \int_0^\pi \frac{1}{\pi}\int_{-\infty}^{\infty} F(t,\theta)\int_{-\infty}^{\infty} f(t\cos\theta - s\sin\theta, t\sin\theta + s\cos\theta)dsdtd\theta.$$

Switch the order of integration to give

$$\langle \mathscr{R}f, F\rangle = \int_{-\infty}^{\infty}\int_{-\infty}^{\infty}\frac{1}{\pi}\int_0^\pi f(t\cos\theta - s\sin\theta, t\sin\theta + s\cos\theta)F(t,\theta)d\theta dsdt.$$

Changing coordinates from $(t,\theta)$ back to $(x,y)$ via the substitutions $x = t\cos\theta - s\sin\theta$ and $y = t\sin\theta + s\cos\theta$, the integral becomes

$$\langle \mathscr{R}f, F\rangle = \int_{-\infty}^{\infty}\int_{-\infty}^{\infty} f(x,y)\frac{1}{\pi}\int_0^\pi F(x\cos\theta + y\sin\theta,\theta)d\theta dxdy.$$

Substitute in the definition of the adjoint $\mathscr{R}^*$ to find

$$\langle \mathscr{R}f, F\rangle = \int_{-\infty}^{\infty}\int_{-\infty}^{\infty} f(x,y)\mathscr{R}^*F(x,y)dxdy = \langle f, \mathscr{R}^*F\rangle,$$

thus exhibiting the equality between the inner product in the Radon transform line integral coordinate system $(t,\theta)$ and an inner product in the traditional planar coordinate system $(x,y)$. □

In order to introduce the inversion formula for the Radon transform, first consider a simple notational convention. For every fixed vector $K=(\kappa,\lambda)$ in the plane, let $f_K$ be the translation of $f$ by $-K$. Therefore $f_K(x,y) = f(x+\kappa, y+\lambda)$. This latter relationship also leads to the fact that

$$\mathscr{R}(f_K)(\xi) = \mathscr{R}f(\xi + K).$$

Proving this assertion requires the use of the Radon transform definition and our new notation, as

$$\begin{aligned}\mathscr{R}(f_K)(\xi) &= \int_{-\infty}^{\infty} f_K(t\cos\theta - s\sin\theta, t\sin\theta + s\cos\theta)dt \\ &= \int_{-\infty}^{\infty} f(\kappa + t\cos\theta - s\sin\theta, \lambda + t\sin\theta + s\cos\theta)dt = \mathscr{R}f(\xi+K).\end{aligned}$$

In order to derive the inversion formula, we will first approximate the function $f(x,y)$ by its average over a small disk $D(X,z)$ of radius $z$ centered at $X=(x,y)$. By the continuity of $f$ assumed in the Radon transform,

$$f(x,y) = \lim_{z\to 0}\frac{1}{\pi z^2}\int\int_{D(X,z)} f(\kappa,\lambda)d\kappa d\lambda.$$

Let $\gamma_z$ be the function equal to $\frac{1}{\pi z^2}$ in the disk of radius $z$ centered at the origin $D(0,z)$ and equal to zero outside this disk. Then

$$f(x,y) = f_X(0,0) = \lim_{z\to 0}\frac{1}{\pi z^2}\int\int_{D(X,z)} f_X(\kappa,\lambda)d\kappa d\lambda = \lim_{z\to 0}\langle f_X, \gamma_z\rangle.$$

Suppose the existence of some function $\Gamma_z$ of $t$ and $\theta$ such that $\gamma_z = \mathscr{R}^*\Gamma_z$. Then

$$f(x,y) = \lim_{z\to 0}\langle f_X, \gamma_z\rangle = \lim_{z\to 0}\langle f_X, \mathscr{R}^*\Gamma_z\rangle = \lim_{z\to 0}\langle \mathscr{R}f_X, \Gamma_z\rangle.$$

When expanded, the rightmost term provides us with a simple and useful formula for the inverse Radon transform $\mathscr{R}^{-1}$ and proves that $f$ is unique.

**Definition 8.2** (from [3]). *The **inverse Radon transform** $\mathscr{R}^{-1}$ recovers a function $f$ from the Radon transform $\mathscr{R}f$ of that function. This inversion is given by the formula*

$$f(x,y) = \lim_{z\to 0}\frac{1}{\pi}\int_0^{\pi}\int_{-\infty}^{\infty}\mathscr{R}f(t - x\cos\theta - y\sin\theta, \theta)\Gamma_z(t)dtd\theta.$$

We must now find a function $\Gamma_z$ that satisfies $\gamma_z = \mathscr{R}^*\Gamma_z$. The function

$$\Gamma_z(t) = \begin{cases} 1/(\pi z^2) & \text{for } -z \le t \le z, \\ \frac{1}{\pi z^2}\left(1 - \frac{1}{\sqrt{1-z^2/t^2}}\right) & \text{for } |t| > z. \end{cases}$$

satisfies this condition. In order to to prove this, move into polar coordinates $(\rho,\phi)$, performing the substitutions $x = \rho\cos\phi$ and $y = \rho\sin\phi$. Here, we can distinguish

between two cases: when $\rho \leq z$ and when $\rho > z$. Consider the former case first. For a line $\ell_{t,\theta}$ through a point $X = (x, y)$,

$$[\mathscr{R}^*\Gamma_z](x,y) = \frac{1}{\pi}\int_0^\pi \Gamma_z(x\cos\theta + y\sin\theta)d\theta = \frac{1}{\pi}\int_0^\pi \frac{d\theta}{\pi z^2} = \frac{1}{\pi z^2} = \gamma_z(x,y).$$

The next case, $\rho > z$, is slightly more complicated. Notice from its equation that $\Gamma_z$ is dependent only on $t$, and in fact on $t^2$–it is independent of the angle $\theta$. Using this in conjunction with the fact that $\cos^2$ has a period of $\pi$, we can make the substitution $\sigma = \theta - \phi$ to find

$$[\mathscr{R}^*\Gamma_z](x,y) = \frac{1}{\pi}\int_0^\pi \Gamma_z(\rho\cos\phi\cos\theta + \rho\sin\phi\sin\theta)d\theta = \frac{1}{\pi}\int_0^\pi \Gamma_z(\rho\cos\sigma)d\sigma.$$

We can once again distinguish two cases: where $|\rho\cos\sigma| \leq z$ and where $|\rho\cos\sigma| > z$. To simplify our integrals slightly, let $\beta = \cos^{-1}\left(\frac{z}{\rho}\right)$. Our first case is now where $\beta \leq \sigma \leq \pi - \beta$, so

$$\frac{1}{\pi}\int_\beta^{\pi-\beta} \Gamma_z(\rho\cos\sigma)d\sigma = \frac{1}{\pi}\int_\beta^{\pi-\beta} \frac{1}{\pi z^2}d\sigma = \frac{\pi - 2\beta}{\pi^2 z^2}.$$

In our second case, where $0 \leq \beta$ or $\pi - \beta < \sigma < \pi$, we can make the substitution $\sin\sigma = \sqrt{1 - z^2/\rho^2}\sin\zeta$, so that

$$\int_0^\beta \frac{d\sigma}{\sqrt{1 - z^2/(\rho^2\cos^2\sigma)}} = \int_0^{\pi/2} d\zeta = \frac{\pi}{2}\left(\cos^{-1}\left(\frac{\sin\sigma}{\sqrt{1 - z^2/\rho^2}}\right)\Bigg|_0^\beta\right).$$

Using this substitution, we find that

$$\begin{aligned}\frac{1}{\pi}\int_0^\beta \frac{1}{\pi z^2}\left(1 - \frac{1}{\sqrt{1 - z^2/\rho^2\cos^2\sigma}}\right)d\sigma &= \frac{\beta - \pi/2}{\pi^2 z^2} \\ &= \frac{1}{\pi}\int_{\pi-\beta}^\pi \frac{1}{\pi z^2}\left(1 - \frac{1}{\sqrt{\frac{1-z^2}{\rho^2\cos^2\sigma}}}\right)d\sigma.\end{aligned}$$

If we add the three components of the second case ($0 \leq \sigma < \beta$, $\beta \leq \sigma \leq \pi - \beta$, and $\pi - \beta < \sigma < \pi$), we find that $[\mathscr{R}^*\Gamma_z](x,y) = 0 = \gamma_z(x,y)$. Therefore, our proposition is true and $\mathscr{R}^*\Gamma_z = \gamma_z$.

## 9. Example: A Simple "Body"

To show the process of a CT scan and reconstruction–the forward and inverse problems associated with the Radon transform–let us consider a simple annulus defined by

$$E(x,y) = \begin{cases} 1 & 1 \leq x^2 + y^2 \leq 4 \\ 0 & \text{everywhere else.}\end{cases}$$

This function is an annulus of height one centered at the origin. If we show $E$ with a binary coloring scheme, where white is equivalent to a value of $E(x,y) = 1$ and black is equivalent to a value of $E(x,y) = 0$, we obtain the image in figure 8. The function $E$ is representative of the "body" imaged in CT scanning. In true CT imaging, the "body" function is an unknown. The known, experimental data in CT scanning is the scan of the body–the *Radon transform* of the function. Therefore, our example does not exactly represent the process of CT scanning and image

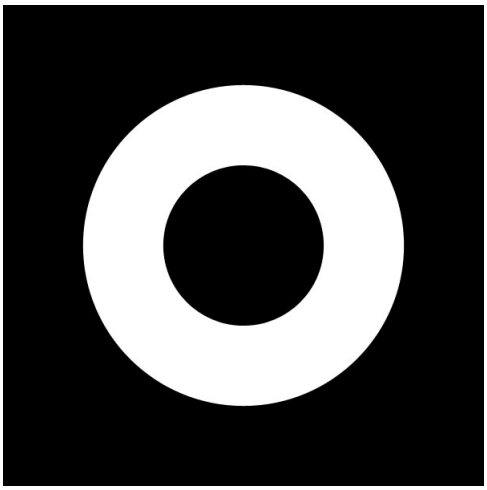

FIGURE 8. The piecewise-defined function $E$.

reconstruction, because the initial body is a known entity from which we determine the Radon Transform instead of the reverse.

The Radon transform of the function $E$ is given by moving into our previously described parametrization by setting $x = t\cos\theta - s\sin\theta$ and $y = t\sin\theta + s\cos\theta$ and putting these new parameters into the Radon transform

$$\mathscr{R}E(t,\theta) = \int_{-\infty}^{\infty} E(t\cos\theta - s\sin\theta, t\sin\theta + s\cos\theta)ds.$$

Performing this integration, we find that

$$\mathscr{R}E(t,\theta) = \begin{cases} 2\left(\sqrt{4-t^2} - \sqrt{1-t^2}\right) & \text{for} \quad |t| \leq 1 \\ 2\sqrt{4-t^2} & \text{for} \quad 1 < |t| \leq 2 \\ 0 & \text{for} \quad 2 < |t|. \end{cases}$$

Graphing this over all values of $t$ and $\theta$ yields the "film image" of the function $E$, the raw data obtained from a CT scan of the "body" $E$, as seen in figure 9.

These graphs of the Radon transform model "raw" CT data obtained from a body scan and illustrate the need for mathematical reconstruction. The Radon transform for this simple function does not give a clear impression of what the function $E$ actually looks like, and makes it impossible to discern any features significant to diagnostic use.

Therefore, in order to use the CT scan diagnostically, we must reconstruct the "body" (the original function $E$) from the Radon transform in figure 9. If we attempt to do this via unfiltered backprojection, we create the image in figure 10. This reconstruction gives a general shape to the data, but it does not maintain any sharp edges and would lose much of the data of a lower-contrast image. If we recall from the introduction that most of the soft tissue imaged with CT differs by only a small fraction (approximately 1%) of the range between air and bone (the "black" and "white" of actual CT imaging) [1], we can see that this reconstruction is simply not specific enough for real-world use.

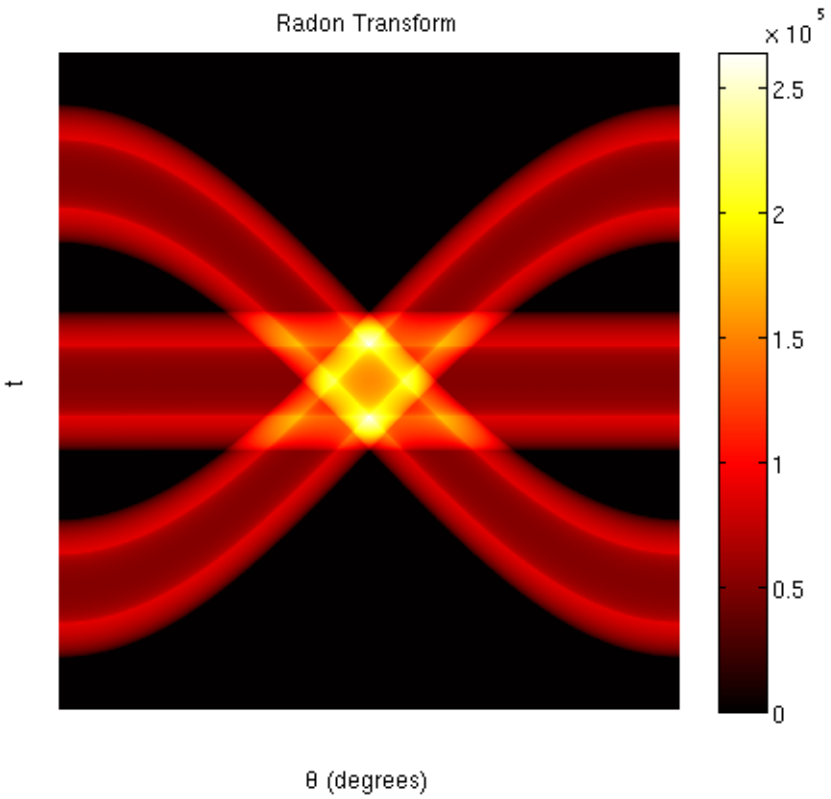


FIGURE 9. The Radon transform of the function $E$, representative of "film" data that would result from a CT scan of $E$. The color scale represents the degree of attenuation of the beam (the "density" of the function $E$). Image created using MATLAB.

In order to do this, we utilize the inverse Radon transform

$$E(x,y) = \lim_{z\to 0} \frac{1}{\pi} \int_0^\pi \int_{-\infty}^\infty \mathscr{R}E(t - x\cos\theta - y\sin\theta, \theta)\Gamma_z(t)dtd\theta,$$

where $\Gamma_z$ is given by

$$\Gamma_z(t) = \begin{cases} 1/(\pi z^2) & \text{for } -z \le t \le z, \\ \frac{1}{\pi z^2}\left(1 - \frac{1}{\sqrt{1-z^2/t^2}}\right) & \text{for } |t| > z. \end{cases}$$

Theoretically, this inversion formula could retrieve the exact function $E$ and perform a completely faithful reconstruction. However, this relies on having data from an infinite number of angles $\theta$, which is impossible in practice. Therefore, the quality of our image reconstructions are highly dependent upon the amount of data we obtain initially. Figure 11 shows how the reconstruction of our function $E$ improves significantly as more and more angles of data are taken. As we go up to 360 and 720 angles (taking measurements every half and quarter degree for a 180° arc, respectively), the reconstruction is indistinguishable from our initial function $E$. For a more complex function, it is possible that more angles would be necessary,

FIGURE 10. The reconstruction of the function $E$ using unfiltered backprojection. Image created using MATLAB.

but this example illustrates the profound improvement in reconstruction as more data is used.

## 10. Conclusions

The Radon inversion is crucial to modern medical imaging technology because it provides the ability to make diagnostically useful reconstructions out of CT scans and other radial imaging. In order to perform this inversion, it is important to understand the mathematics of the forward Radon transform and its connection via the Central Slice Theorem to the well-studied Fourier transform and its inversion.

Inversion of the Radon transform should be performed with the inverse Radon transform (filtered backprojection) to avoid the blurring artifacts and lack of clarity in unfiltered backprojection. Clarity is vital to an effective Radon reconstruction because the main targets of CT investigation–soft tissues–are only subtly different. The application of the inverse Radon transform must also take this issue into account, as the amount of discrete data collected by an initial CT scan has a profound effect on the clarity of the resulting reconstruction.

An interesting problem for the present and future is how to balance a need for spatial clarity for diagnostic usefulness while constraining patient radiation exposure. This is not only a pragmatic question, but an ethical and mathematical one. How much future risk should a patient be exposed to in order to treat a current ailment? Mathematically, what methods can be used to reduce the level of radiation exposure required to achieve the same levels of diagnostic accuracy? Current studies apply neural network techniques to create computer-assisted diagnostic tools [4]. Studies on a related technique, diffuse optical tomography, apply model reduction and approximation error techniques to lower the number of discrete measurements required for accurate reconstructions [5, 6]. Other investigations use algebraic reconstruction techniques to lower the computation required in CT reconstruction [7]. These novel techniques all present interesting new perspectives on this problem

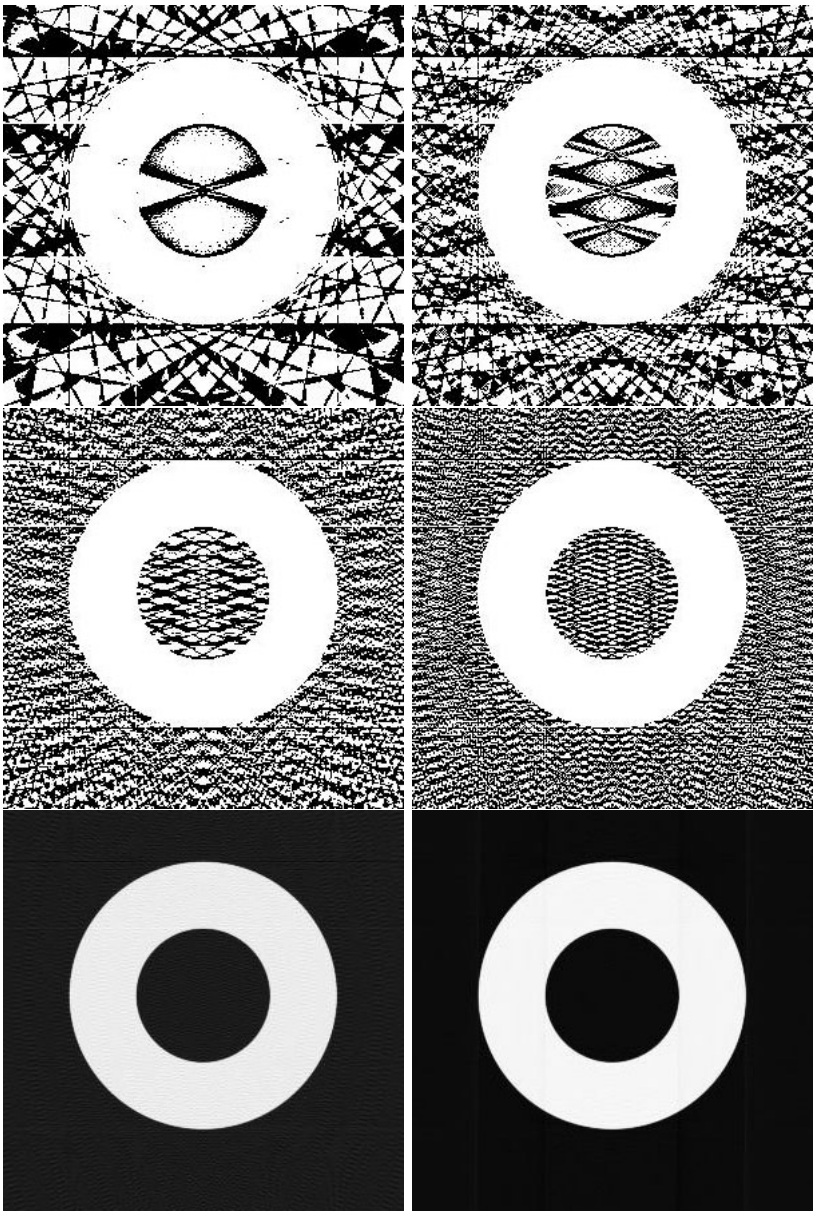

FIGURE 11. Inverse Radon transform $\mathscr{R}^{-1}(E)$ reconstructions of the piecewise-defined function $E$ using 18, (upper left), 36 (upper right), 90 (middle left), 180 (middle right), 360 (lower left), and 720 (lower right) discrete angles $\theta$ along a 180° arc around the "body". Images created using MATLAB.

that would be both possible and valuable to investigate further, so that the application of CT scanning can be better optimized to provide effective and safe viewing of the body.

## References

[1] Epstein, Charles L. *Introduction to the Mathematics of Medical Imaging*. 2nd ed. Philadelphia, PA: Society for Industrial and Applied Mathematics, 2008. Print.

[2] O'Neil, Peter V. *Advanced Engineering Mathematics*. 5th ed. Toronto: Thomson, 2007. Print.

[3] Nievergelt, Yves. Elementary Inversion of Radon's Transform. *SIAM Review*, Vol. 28, No. 1 (Mar., 1986), pp. 79-84.

[4] Suzuki, K.; Feng Li; Sone, S.; Doi, K. Computer-aided diagnostic scheme for distinction between benign and malignant nodules in thoracic low-dose CT by use of massive training artificial neural network. *IEEE Transactions on Medical Imaging*, Vol. 24, No. 9 (Sept., 2005), pp. 1138-1150.

[5] Kolehmainen, V; Schweiger, M; Nissila, I; Tarvainen, T; Arridge, S; Kaipio, J. Approximation errors and model reduction in three-dimensional diffuse optical tomography. *J. Opt. Soc. Am. A.*, Vol. 26, No. 10 (Oct., 2009), pp. 2257-2268.

[6] Tarvainen, T; Kolehmainen, V; Pulkkinen, A; Vauhkonen, M; Schweiger, M; Arridge, S; Kaipio, J. An approximation error approach for compensating for modelling errors between the radiative transfer equation and the diffusion approximation in diffuse optical tomography. *Inverse Problems*, Vol. 26 (Dec., 2009).

[7] Bal, Guillame. Fast numerical inversion of the attenuated radon transform with full and partial measurements. *Inverse Problems*, Vol. 20 (May, 2004), pp. 1137-1164.